processes

MDPI

Article

Study on the Relationship between Wear and Flow Characteristics of a Centrifugal Pump at Different Mass Concentrations

Zhongqian Jiang, Xiaodong Zeng and Yi Li *

State-Province Joint Engineering Lab of Fluid Transmission System Technology, Zhejiang Sci-Tech University, Hangzhou 310018, China; jiangzhongqian@outlook.com (Z.J.); zeng-xiaodong@hotmail.com (X.Z.)
* Correspondence: liyi@zstu.edu.cn; Tel.: +86-1364-684-6259

Abstract: In order to study the wear characteristic of a centrifugal pump at different mass concentrations, simulation and experimental research were carried out. The simulation was based on the DPM (discrete phase model) to complete the coupling of particles and the flow field. The experimental research included a performance test and a wear test. Through the comparison of the simulation and experimental research results, the relationship between the particle movement and the wear was analyzed, and the flow field was analyzed through the energy gradient theory. The energy gradient and the particle movement were combined to explain the wear characteristics. When the particles entered the impeller flow area, they directly hit the leading edge of the blade and the hub wall. The particles were sinking due to the flow field, which caused the particles to accumulate near the hub and the pressure surface. These places were at the most severely worn wall. The farther away from the axis the position was, the greater the relative velocity difference between the particles and the wall was, so that wear occurred first in these places. The low-energy properties near the hub made particles gather there, which was also the most serious cause of hub wear.

Keywords: centrifugal pump; large particle; wear characteristics; energy transport; solid–liquid two-phase flow

check for updates

Citation: Jiang, Z.; Zeng, X.; Li, Y. Study on the Relationship between Wear and Flow Characteristics of a Centrifugal Pump at Different Mass Concentrations. *Processes* **2021**, *9*, 988. https://doi.org/10.3390/pr9060988

Academic Editor: Farhad Ein-Mozaffari

Received: 16 April 2021
Accepted: 1 June 2021
Published: 3 June 2021

1. Introduction

In industrial applications, when a centrifugal pump performs solid–liquid two-phase transportation, the collision between the rotating blades and the particles causes wear on the wall of the centrifugal pump flow passage, which has a great impact on the service life of the centrifugal pump. However, due to the complexity of the flow passage of a centrifugal pump and the diversity of the solid–liquid two-phase flow, it is difficult to study the internal wear of a centrifugal pump. Therefore, although many scholars have carried out a lot of research on this topic, the law of wear inside a centrifugal pump has not been well-revealed.

Khalid et al. [1] put a centrifugal pump impeller into a cylinder containing a mixture of sand and water and made the impeller spin. Through the method of thickness and weighing measurement, the relationship between the wear of the centrifugal pump impeller and time was determined, and it was found that the mass loss of the impeller had a linear relationship with the wear time. Wang et al. [2] conducted experiments on double suction centrifugal pumps to study the changes in the hydraulic performance by controlling the size and concentration of the conveyed particles, and Wang proposed a corresponding functional relationship by processing the experimental data, which was of great help to pump manufacturing. Ravelet et al. [3] conducted an experimental study on the hydraulic transportation of large solid particles above 5 mm in horizontal pipes. The experimental results were compared with a one-dimensional model based on mass and momentum balance, and a flow model for large particles in vertical pipes was proposed. Zouaoui [4] experimentally studied the flow of large particles in a horizontal pipe by varying the particle material, particle size, and concentration to test important parameters (pressure, velocity, and others) during the transport of solids. The results showed that the relationship between the pressure gradient force and the mixing velocity was significantly different from that of pure liquid flow. Zhao et al. [5] used the shear stress transport (SST) k-ω turbulence model to simulate the transient process of the three-dimensional flow in a centrifugal pump. The simulation results showed that the solid-phase particle concentration had a strong influence on the external characteristics and turbulent kinetic energy of the centrifugal pump. At the same time, the particle size had a certain effect on the flow field in the centrifugal pump, but this effect was not directly proportional to the particle size. Qian et al. [6] analyzed the wear data of a double-suction centrifugal pump and found that the wear of the blade inlet and outlet was very serious, and the average wear rate of the suction surface of the blade was higher than that of the pressure surface. Through further analysis, it was concluded that the impact velocities of the entrance, exit, and impact angle were important factors affecting the wear rate. Pagalthivarthi et al. [7] studied the wear of the volute when a centrifugal pump delivered low-concentration slurry based on the DPM model, and they qualitatively described the influence of the geometric parameters of the centrifugal pump on the wear performance. Shen et al. [8] used the DPM model to simulate the wear of a centrifugal pump with the particle diameter and the particle volume fraction, and found that the volume fraction of large-diameter particles seriously affected the movement trajectory of the particles. Moreover, particles with large diameters were more likely to produce velocity slip than particles with small diameters. Tarodiya et al. [9] used a mud centrifugal pump to carry out a research method combining experiment and numerical simulation. The study focused on the relationship between the volute wear law and the flow field as well as the wear mechanism. Kaushal et al. [10] used the mixed model and the Euler two-phase model to numerically simulate the flow of high-concentration particle slurry in a pipeline, predict the pressure drop in the pipeline, and analyze the distribution of the velocity and concentration in the pipeline. Huang et al. [11] conducted research about the low wear in the simulation under the condition of different flow rates. It was found that as the flow rate increases, the wear in the blade pressure side and the hub increases significantly. Cai et al. [12] explained the wear pattern and mechanism of centrifugal pumps using vorticity and the Q-Criterion as variables, rationalized the wear characteristics of an impeller, and optimized the impeller. The results showed that the impeller wear could be reduced by reducing the efficiency and head by a small amount.

Based on the above research results, it can be found that the trajectory of large particles in a flow passage is quite different from that of small particles, so the wall wear is different. However, the existing centrifugal pump wear studies have mostly been carried out for the solid–liquid two-phase flow of small particles. In this study, experiments and numerical simulations were carried out on centrifugal pumps that transported large particles in solid–liquid two-phase flow to study particle movement and wear in the impeller channel, and at the same time, introduce the energy gradients method to analyze flow field characteristics and analyze their relationship with particle aggregation. The results can provide references for the wear optimization of centrifugal pumps.

2. Experiment and Simulation

2.1. Experiment Project

An experimental system was built in this research. The experimental system is shown in Figure 1. This system includes an experimental centrifugal pump, a pipeline pump for inlet pressurization to prevent cavitation, two pressure sensors for measuring inlet and outlet pressures, an electromagnetic flowmeter for measuring flow rate, a water tank for storing solid–liquid two-phase flow, an agitator for mixing two-phase flow, a filter sieve to prevent particles from sinking into the drainage pipe, a torque sensor for measuring shaft torque and rotating speed, a drain valve for draining water, an inlet valve used to control the start of the experiment, and an outlet valve to control the flow rate.

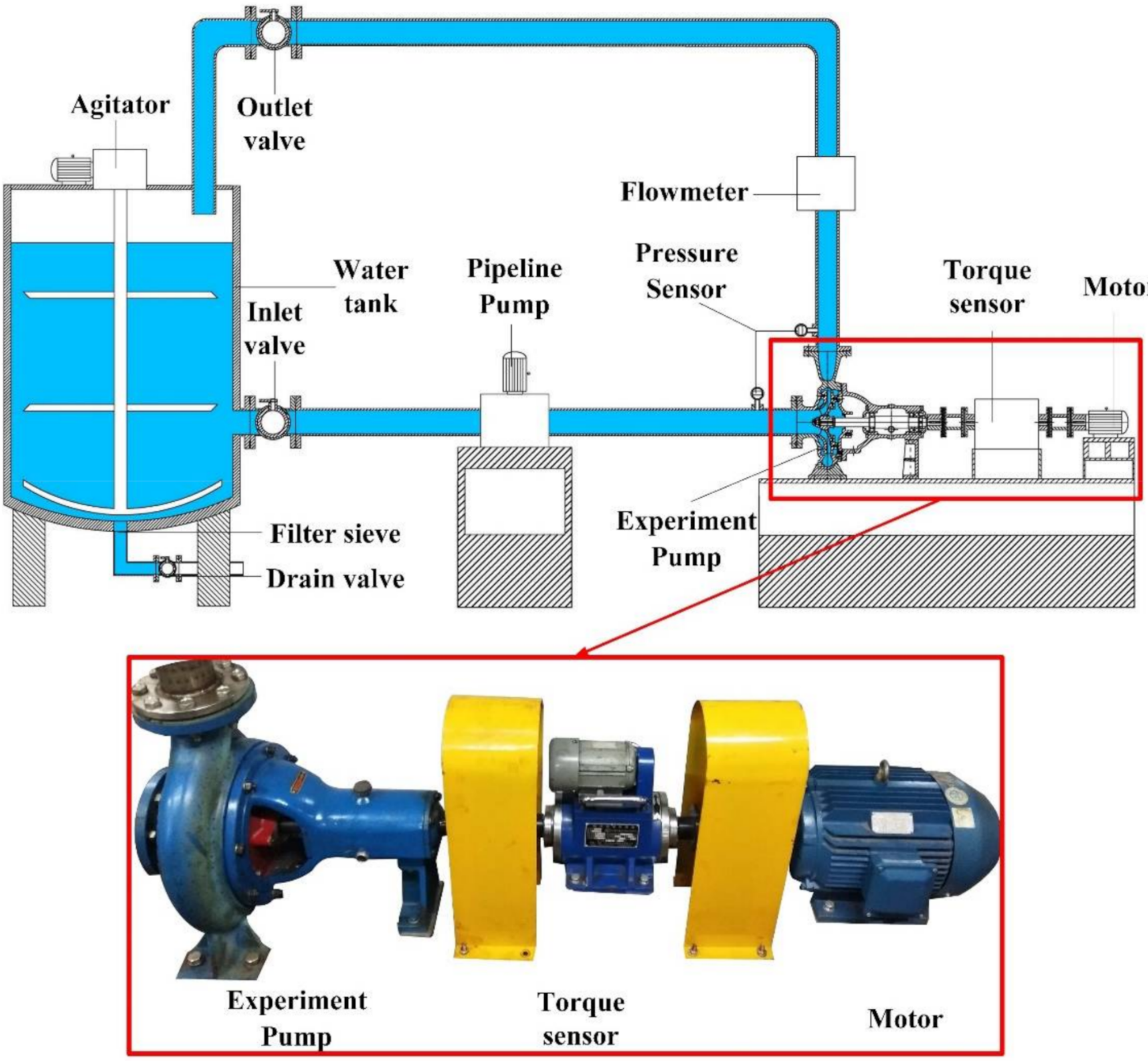

Figure 1. Experimental system.

The centrifugal pump used in the experiment was model HCK100-80-250, the rated flow was 70 m^3/h, the head was 14 m, the rotating speed of impeller was 1450 r/min, and the specific speed was 102. The centrifugal impeller was a three-blade fully open impeller, the impeller inlet diameter was 108 mm, and the outlet diameter was 265 mm. The front and rear wear plates of the experimental pump were removable. The surfaces on the centrifugal pump impeller were painted with a layer of blue paint, which could be used to identify the wear area of the impeller.

The particle material used in the experiment consisted of round glass balls with a density of 2700 kg/m^3, a diameter of 3 mm, and a hardness of 6.5 Mohs. In the wear experiment, particle mass concentrations were 1%, 2%, 3%, 4%, 5%, and 6%, respectively. Before the wear experiment started, the quality of the water in the tank was first measured: the volume could be determined according to the ruler on the tank, and then the quality of water could be calculated. Then, according to the particle mass fraction in the research plan, the mass of particles at different concentrations were calculated. Before each experiment, the particles of the corresponding quality were put into the water tank, and then the agitator was turned on to make the particles evenly mixed during the experiment. Then, the pipeline pump was turned on. A container was used to collect the two-phase flow in the outlet within a certain period of time to calculate the mass concentration. If the deviation between this mass concentration and the set concentration was large, the amounts of particles would be increased appropriately to ensure that the concentration is correct before starting the experiment. The flow rate was adjusted by the valve opening. Each wear experiment time was 48 h.

2.2. Simulation Setting

In this study, Fluent 16.0 was used to complete the numerical simulation of the solid–liquid two-phase flow inside the centrifugal pump. The calculation was based on the DPM model to consider the interaction between the flow field and the solid particles. The flow field was regarded as a continuous phase and the particles were regarded as a discrete phase. The DPM model not only considered the interaction between the particles and the fluid, but also considered the collision and wear between the particles and the wall.

The equation of motion describing the conservation of momentum of a viscous incompressible fluid is the Navier–Stokes equation, expressed in a rectangular coordinate system as:

$$\rho(\frac{\partial u}{\partial t} + u\frac{\partial u}{\partial x} + v\frac{\partial u}{\partial y} + w\frac{\partial u}{\partial z}) = f_x - \frac{\partial P}{\partial x} + (\mu + \mu_t)(\frac{\partial^2 u}{\partial x^2} + \frac{\partial^2 u}{\partial y^2} + \frac{\partial^2 u}{\partial z^2}), \quad (1)$$

$$\rho(\frac{\partial v}{\partial t} + u\frac{\partial v}{\partial x} + v\frac{\partial v}{\partial y} + w\frac{\partial v}{\partial z}) = f_y - \frac{\partial P}{\partial y} + (\mu + \mu_t)(\frac{\partial^2 v}{\partial x^2} + \frac{\partial^2 v}{\partial y^2} + \frac{\partial^2 v}{\partial z^2}), \quad (2)$$

$$\rho(\frac{\partial w}{\partial t} + \frac{\partial w}{\partial x} + \frac{\partial w}{\partial y} + \frac{\partial w}{\partial z}) = f_z - \frac{\partial P}{\partial z} + (\mu + \mu_t)(\frac{\partial^2 w}{\partial x^2} + \frac{\partial^2 w}{\partial y^2} + \frac{\partial^2 w}{\partial z^2}), \quad (3)$$

where, ρ is the fluid density, P is the pressure, u, v, and w are the velocity components of the fluid at the point (x, y, z) at time t, f is the external force per unit volume of the fluid, and the constant μ is the dynamic viscosity and μ_t is the turbulence viscosity.

The turbulence model uses the SST (shear stress transport) model under the turbulence model. Compared with the standard k-ω model, the SST model introduces the damping cross-diffusion derivative term in the specific dissipation rate equation, and modifies the definition of turbulent viscosity. It has high accuracy for moderate separation of turbulence.

The transport equations are:

$$\frac{\partial}{\partial t}(\rho k) + \frac{\partial}{\partial x_j}(\rho k u_i) = \frac{\partial}{\partial x_j}(\Gamma_k \frac{\partial k}{\partial x_j}) + \widetilde{G}_k - Y_k + S_k, \quad (4)$$

$$\frac{\partial}{\partial t}(\rho \omega) + \frac{\partial}{\partial x_j}(\rho \omega u_j) = \frac{\partial}{\partial x_j}(\Gamma_\omega \frac{\partial \omega}{\partial x_j}) + G_\omega - Y_\omega + D_\omega + S_\omega, \quad (5)$$

In these equations, $\widetilde{G}_k$ represents the generation of turbulence kinetic energy due to mean velocity gradients, G_ω represents the generation of ω, Γ_k and Γ_ω represent the effective diffusivity of k and ω respectively, Y_k and Y_ω represent the dissipation of k and ω due to turbulence, D_ω represents the cross-diffusion term, and S_k and S_ω are user-defined source terms.

The collision model was solved with the model proposed by Grant et al. [13], and its expression is:

$$e_n = 0.993 - 1.76\theta_1 + 1.56\theta_1^2 - 0.49\theta_1^3, \quad (6)$$

$$e_t = 0.988 - 1.66\theta_1 + 2.11\theta_1^2 - 0.67\theta_1^3, \quad (7)$$

where, e_n is normal collision elastic recovery coefficient, e_t is tangential collision elastic recovery coefficient, and θ_1 is the collision angle.

The wear model proposed by Ahlert [14] was selected according to the flowing wall medium, and its expression was:

$$ER = \mathrm{A}(BH)^{-0.59} F_s u_p^{n_a} f(\theta), \quad (8)$$

$$f(\theta) = \begin{cases} a\theta^2 + b\theta & \theta \le \theta_0 \\ x\ \cos^2\theta \sin(w\theta) + y\ \sin^2\theta + z & \theta > \theta_0 \end{cases}, \tag{9}$$

where, ER is the wall erosion, A is the constant related to the wall material, BH is the Brinell hardness of the wall material, F_s is the correlation coefficient with the particle shape (the particle is spherical and takes 0.2, and the sharp particle is 1), u_p is the particle collision velocity, and $f(\theta)$ is the particle collision angle function. The selected parameters in the equations is shown in Table 1 according to the wall material.

Table 1. The parameters in the Ahlert wear model.

A	n_a	θ_0	a	b	x	y	z	w
1.599×10^{-7}	1.73	$\pi/12$	−38.4	22.7	3.147	0.3609	2.532	1

The particle motion equation is:

$$m_p \frac{du_p}{dt} = m_p g + F_{drag} + F_p + F_v \tag{10}$$

where m_p is the quality of particles, u_p is the velocity of particles, F_{drag} is the drag force, F_p is the pressure gradient force, and F_v is the additional mass force.

In the simulation, the inlet boundary condition was velocity inlet, which was set to 2.47 m/s, and this velocity was calculated by rated flow and inlet diameter. In order to observe the fully developed internal flow, the corresponding turbulence parameters on the boundary conditions were set, which are the turbulence intensity (I = 0.0339073059070281) and the hydraulic diameter (100 mm). The file form was selected for particle injection on the inlet surface, and 64 particle injection points were evenly distributed on the inlet surface. The particle inject speed is the same as the fluid of 2.47 m/s. This velocity was considered to have the same velocity as the flow. The impeller zone condition used mesh motion and the rotating speed was set to 1450 r/min, which was same rotating speed as the centrifugal pump impeller in the experiment. The outlet boundary condition was outflow. The collision model and the wear model in the wall of impeller and volute were the model mentioned above. The setting of all boundary conditions in the simulation was determined based on experimental conditions. Under this condition, time step was set to 0.00011494255 s, which was the time of the impeller to rotate through 1°, and the convergence criterion of the residual value in each time step was set to 10^{-4}. The simulation was considered complete when the number of particles in the centrifugal pump gradually stabilized.

2.3. Grid Setting

The entire model and grid of the experimental pump are shown in Figure 2. The solid–liquid two-phase fluid entered the impeller flow area through the inlet pipe, then entered the volute after being accelerated by the rotation of the impeller, and finally flowed out from the outlet of the volute.

In order to meet the calculation requirements, the minimum angle of the generated grid was 24°, and the minimum quality of the grid was 0.3. In order to eliminate the influence of the number of grids on the results of the simulation, a total of 8 sets of grids were generated, and the number of nodes gradually increased from 460,426 to 3,561,073. The calculation and the analysis of the internal flow of the centrifugal pump are shown in Table 2.

By comparing the heads, it could be seen that the head values remained almost unchanged starting from the fifth set of grids, indicating that the number of grids had nothing to do with the calculation results. Therefore, in order to ensure the accuracy of the simulation, the sixth set of grids was selected for numerical simulation.

2.4. Simulation Accuracy Verification

In order to verify the accuracy of the calculation method and the simulation results, the simulated performance of the centrifugal pumps with different particle mass concentrations (0–6%) was compared with the experimental performance for the design flow of 70 m^3/h.

The head, power, and efficiency of the centrifugal pump were calculated as follows. The variables in the equations were measured by the measuring instruments in the experimental system.

$$H = \frac{P_{out} - P_{in}}{\rho g} + \frac{{V_{out}}^2 - {V_{in}}^2}{2g} + Z_{out} - Z_{in}, \tag{11}$$

$$P_w = T\omega \times 10^{-3} = \frac{T \times 2\pi n}{60000} = \frac{Tn}{9550}, \tag{12}$$

$$\eta = \frac{\rho g Q H}{P_w}, \tag{13}$$

where, H is the head, P_w is the power, η is the efficiency, P_{out} is the pressure of outlet, P_{in} is the pressure of inlet, V_{out} is the velocity of outlet, V_{in} is the velocity of inlet, Z_{out} is the height of outlet, Z_{in} is the height of inlet, T is the torque, and n is the rotating speed.

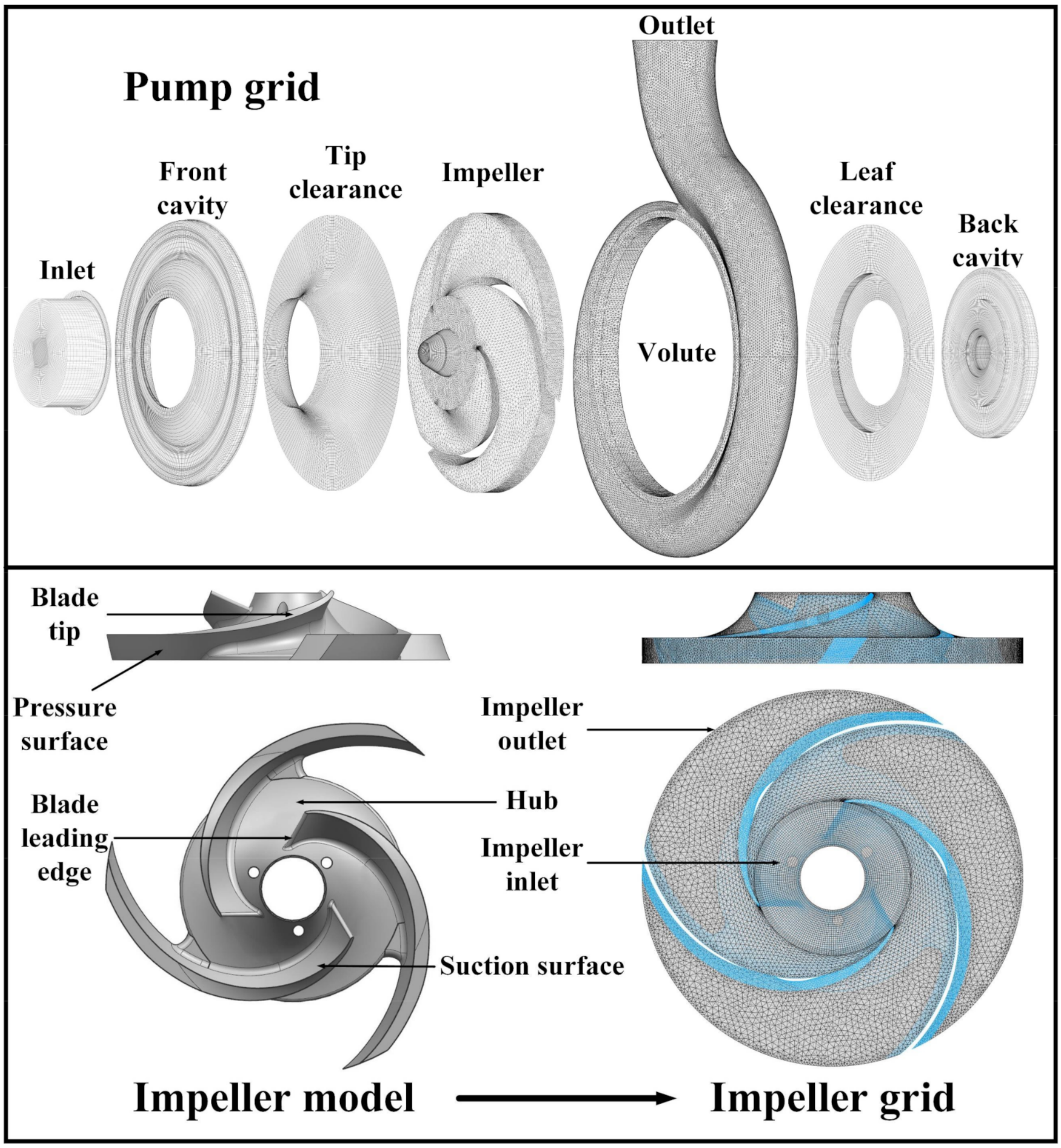

Figure 2. The whole grid, the model, and the grid of the impeller.

Table 2. The number of nodes with the head of each set.

Serial Number of Grid	Number of Nodes	The Head of Simulation
1	460,426	15.28343
2	846,013	15.32418
3	1.1064×10^6	15.28373
4	1.55974×10^6	15.2492
5	2.00676×10^6	15.19412
6	2.42731×10^6	15.19312
7	2.93915×10^6	15.18951
8	3.56107×10^6	15.18709

Figure 3 shows the performance experiment of centrifugal pump under the water condition. From comprehensive design parameters and experimental results, it was found that the design flow point and the experimental best efficiency point basically coincide, that is, 70 m^3/h. The working condition of this centrifugal pump, HCK 100-80-250, in the manuscript is the rated flow in actual application. This study tries to find some rules as a reference for the service life of the centrifugal pump. Therefore, based on this reason, the relationship between the wear characteristics of centrifugal pumps and the internal flow characteristics is explored.

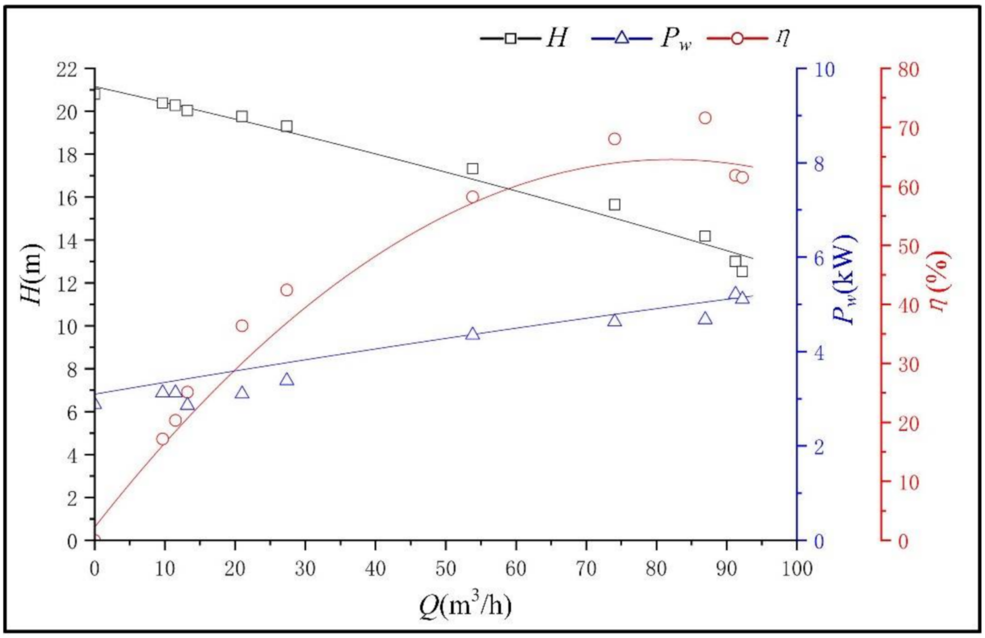

Figure 3. The performance of the pump in the water condition.

In Figure 4, the uncertainties of the performance experimental data were checked. The maximum percentage random uncertainties of flow rate, head, power, and efficiency were 0.75%, 1.64%, 1.47%, and 1.73%, respectively. It can be considered that the experimental results were reliable. The performance obtained with the simulation was slightly higher than the experimental values, and the error was generally less than 5%. Therefore, the calculation method used could be used for the simulation of the solid–liquid two-phase flow inside the centrifugal pump.

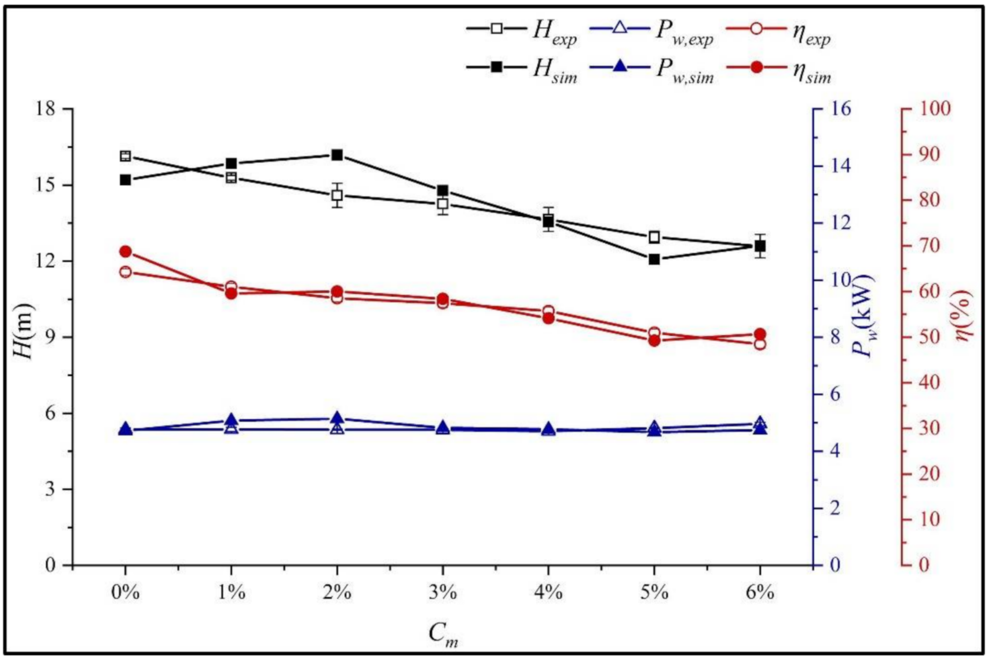

Figure 4. The performance comparison of the experiment and the simulation.

In Figure 4, the subscripts exp and sim represent the power of the experimental result and the simulated result, respectively.

3. Analysis of Results

3.1. Analysis of Wear Results

After the centrifugal pump has undergone 48 h of the solid–liquid two-phase flow abrasion experiment, the internal flow passage of the centrifugal pump has different degrees of wear. Analyzing the results of the wear experiment, it was found that the most severely worn parts in the impeller flow passages are the hub wall and the leading edge of the blade. Under different mass concentration conditions, the hub wall wear is shown in Figure 5.

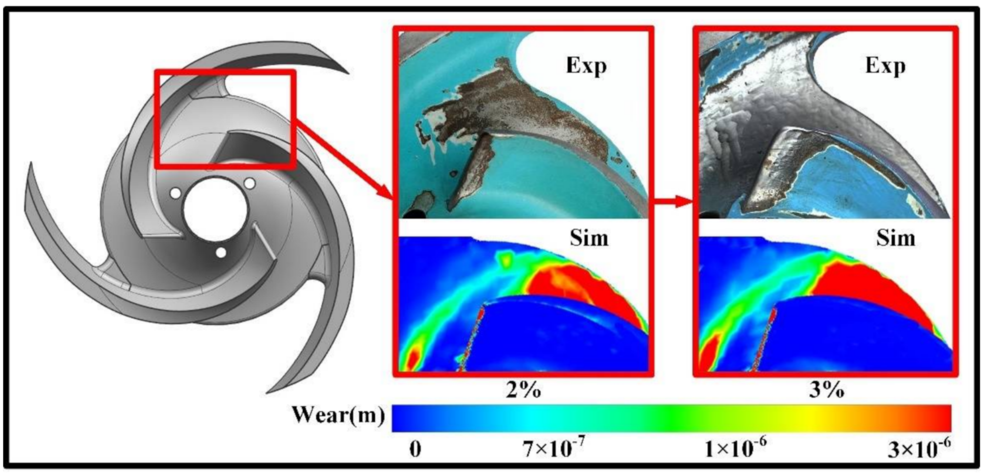

Figure 5. Wear of impeller hub wall at different particle concentrations.

Based on the wall wear results obtained from the experiment and simulation shown in Figure 5, it was obvious that when the centrifugal pump performed the solid–liquid mixed transportation of different concentrations, the wall of the hub near the exit of the impeller flow passage first produced wear, and the wear at this place caused the paint surface to disappear first, exposing the metal surface of the hub wall. It can be found that when the particle mass concentration increased from 2% to 3%, the paint on the wall of the hub disappeared gradually, and the amount of wear also increased, which indicated that the wear range and the wear degree were closely related to the particle concentration. This phenomenon occurs in both simulations and experiments. With further observation of the wear on the wall of the hub, we found that the wear surface had corrugated stripes, which were very similar to the striped wear shown on the wall of the elbow [15].

In order to study the cause of the wear of the hub, the solid–liquid two-phase flow inside the region was analyzed. Since the impeller used in this study was a double-curvature blade, in order to be able to show its internal flow characteristics, the impeller's rotating flow area was expanded into a blade-to-blade region. The diagrams of the blade-to-blade region shown below in Figure 6 at different positions were numbered by the span value, from 0 to 1, representing the blade tip to the root; that is, the smaller the span value was, the closer the position was to the blade tip.

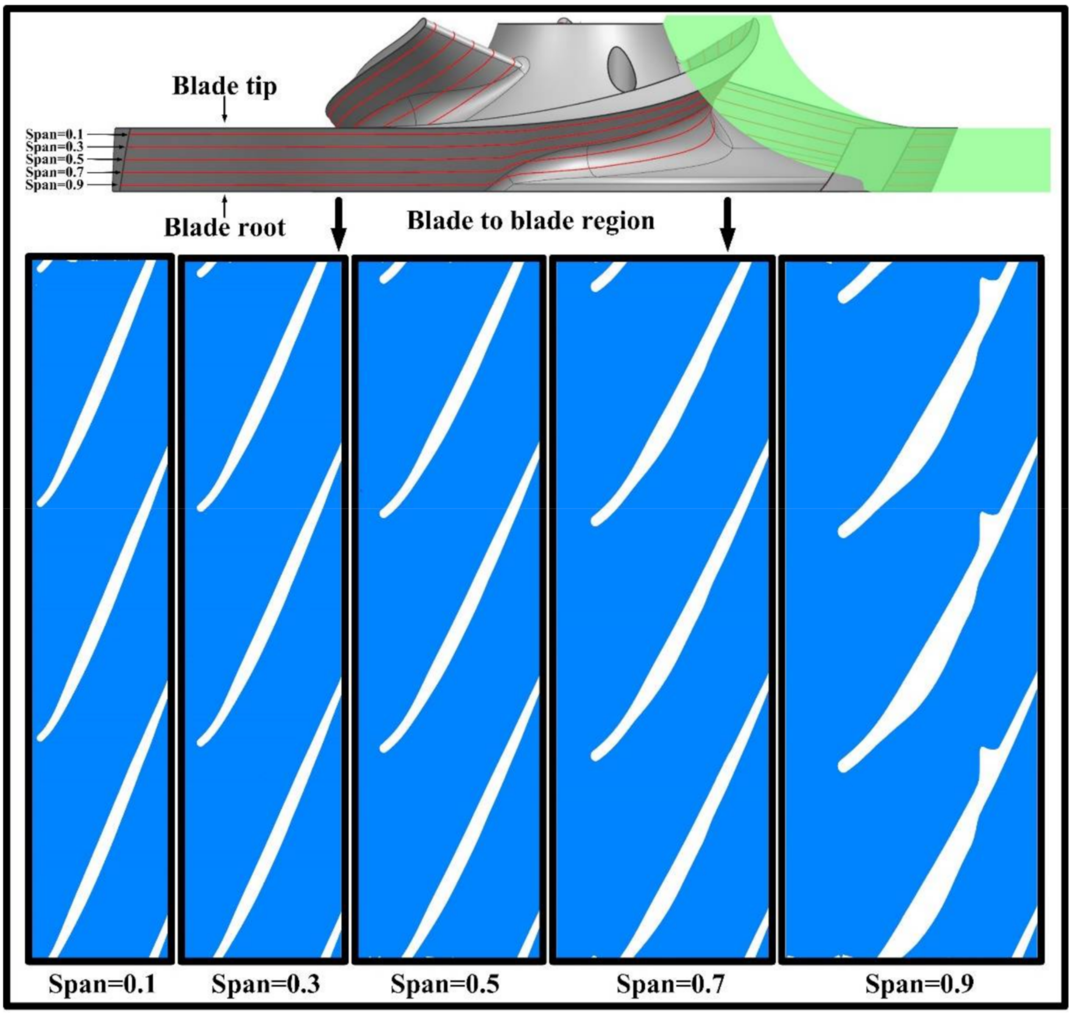

Figure 6. Blade-to-blade region of impeller.

The effect of the presence of solid particles on the flow was studied to investigate the wall wear law by analyzing the flow inside the impeller when the centrifugal pump conveyed water and the solid–liquid two-phase flow. Figure 7 shows the flow and velocity diagrams on the impeller grid expansion surface (Span = 0.9) near the hub area.

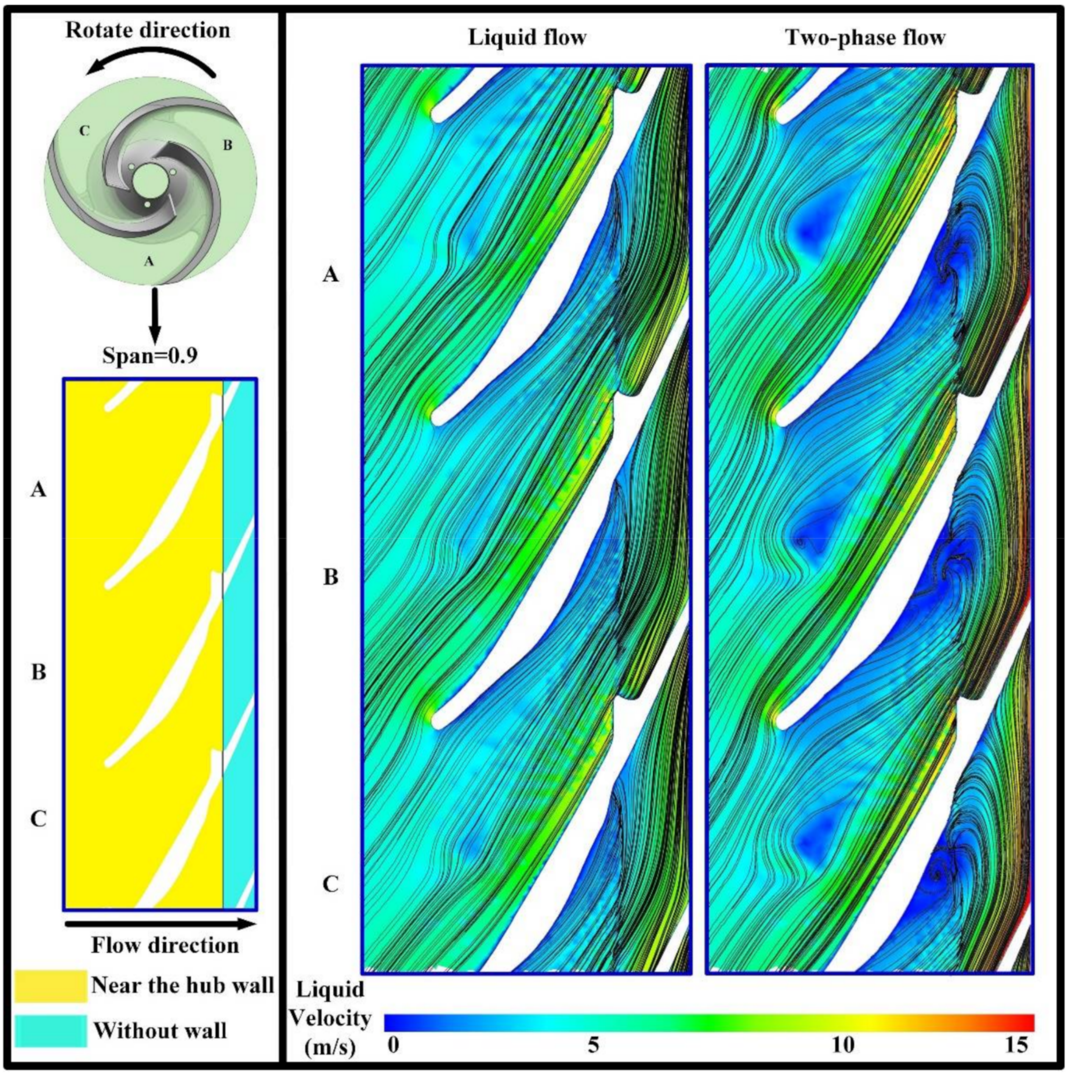

Figure 7. Streamlines and velocity distribution near the hub wall (Span = 0.9).

As can be seen from Figure 7, in the liquid flow condition, the streamline in the area near the hub wall was smooth, the velocity distribution was relatively uniform, and there was no obvious vortex. However, in the solid–liquid two-phase flow condition, there were several low-speed areas in the impeller flow passage, and the flow velocity near the outlet increased with the appearance of the vortex, which corresponded to the earliest disappearance of the hub outlet position in the wear experiment. That is, the fast-flowing fluid entrained the solid particles to rotate and rub at that location, and then wear first occurred in this part. The greater the concentration was, the greater the number of particles was, and the greater the degree of wear and the range of wear were.

Combining the particle motion vector diagram could further reveal the cause of the wheel hub wall wear, as shown in Figure 8.

It can be seen from Figure 8 that after entering the impeller flow area through the inlet pipe, a large number of particles did not collide with any surface to decelerate, but rather directly impacted the wall surface of the impeller hub. Therefore, severe wear occurred at this position first.

It can also be observed from Figure 8 that after the particles entered the impeller flow channel, the wall of the impeller hub was impacted by the particles, and the leading edge of the blade was directly impacted by a large number of particles, as shown in Figure 9.

Therefore, the blade leading edge of the impeller was also severely worn. The experimental and calculated wear results are shown in Figure 10.

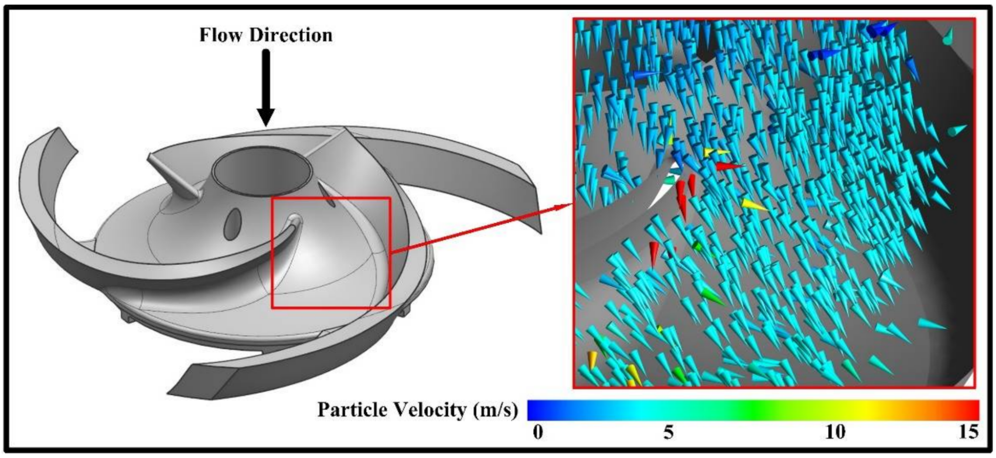

Figure 8. Particle motion vector diagram in the area near the hub wall.

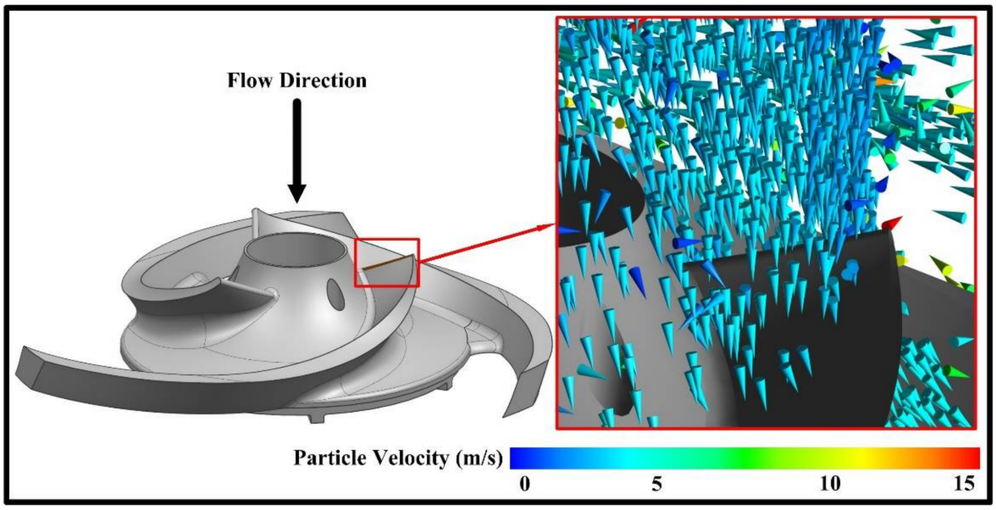

Figure 9. Particle motion vector diagram in the area near the leading edge of the blade.

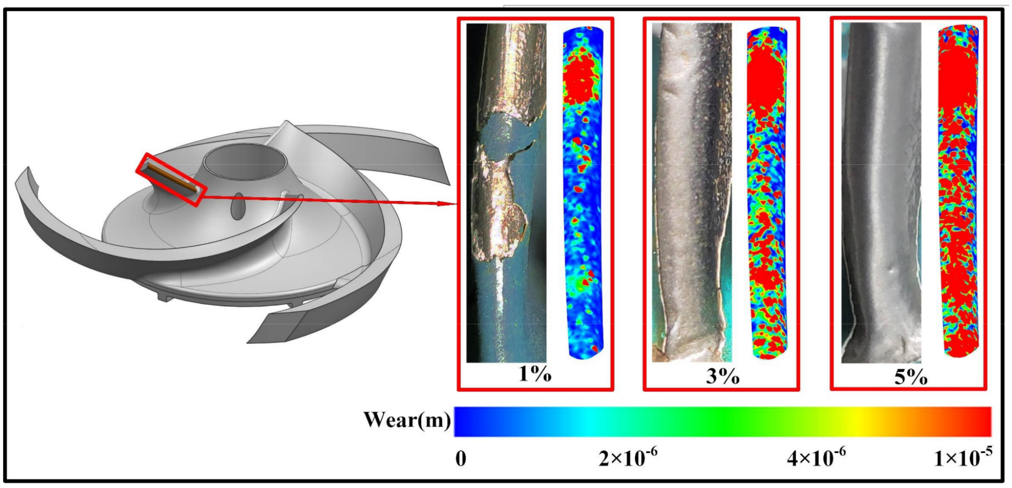

Figure 10. The wear area of the blade leading edge.

It can be clearly seen from Figure 9 that when the particles entered the impeller flow area, the leading edge of the blade was directly impacted by a large number of particles. It can be seen from Figure 10 that after 48 h of abrasion testing at 1% concentration, the paint peeled off on part of the leading edge of blade, while the remaining part of the paint surface remained intact. There were many small pits on the leading edge of the blade. The wear condition was basically consistent with the results obtained by the simulation calculation, and the wear type was mainly impact wear. As the concentration increased, the wear area increased and the degree of wear continued to deepen, but the types of wear were essentially the same. For the case of 3% concentration, the leading edge of the blade was impacted by particles and it disappeared, and at the same time, dents appeared in the blade leading edge. This might have been caused by the continuous impact of particles. At 5% concentration, the leading edge of the blade became smoother, the paint on the blade leading edge was completely peeled off, and a certain degree of distortion appeared.

As the particle concentration increases, it could be seen that the wear degree in the leading edge of the blade area increases, while the wear area expands accordingly. After the paint disappeared completely, pits gradually appeared on the leading edge of the blade. As the concentration further increased, the leading edge of blade gradually became smooth and rounded, and even deformed.

When the liquid phase drove the solid particles to continue to move, they entered the rotating impeller channel through the blade leading edge of the impeller and the hub, and then the particles and fluid rotated under the action of the impeller. The wear of the blade pressure surface is shown in Figure 11.

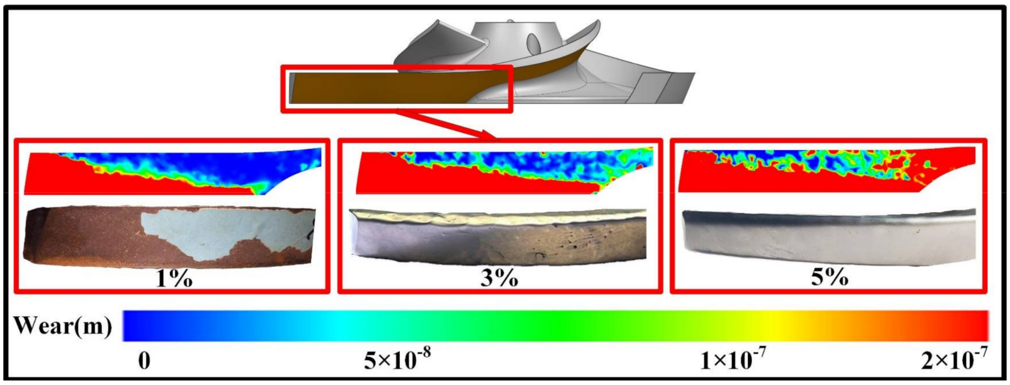

Figure 11. The wear of the blade pressure surface.

It can be seen from Figure 11 that the indicating paint on the pressure surface was only retained for the working condition of 1% concentration, and the indicating paint surface of the pressure surface disappeared completely for the conditions of other concentrations. At the same time, the pressure surface wear trend in the experiment was consistent with the simulation.

The wear of the pressure surface appeared from the root and tail of the pressure surface and then gradually spread to the entire pressure surface. It could be seen that the paint on the pressure surface disappeared completely in the condition of 3% concentration, and the pressure surface was worn smoother for 5% than other concentrations.

From the leading edge of the blade to the tail of the blade, we took a line in the middle of the blades and divided it with 12 points, and named the monitoring points from 1 to 12 in the direction of the arrow, and the thickness loss of the impeller was measured at these monitor points. Figure 12 shows the monitoring point on a blade and the mark of the impeller blade.

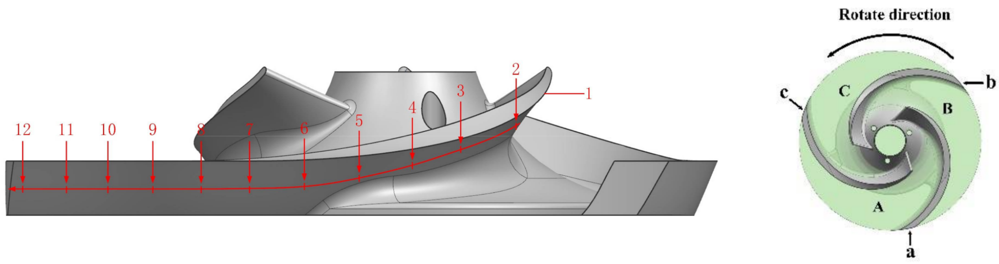

(**a**) (**b**)

Figure 12. (**a**) The monitor points on the blade, and (**b**) The mark of the impeller blade.

Figure 13 shows the wall thickness loss at 1% concentration in the experiment and the simulation.

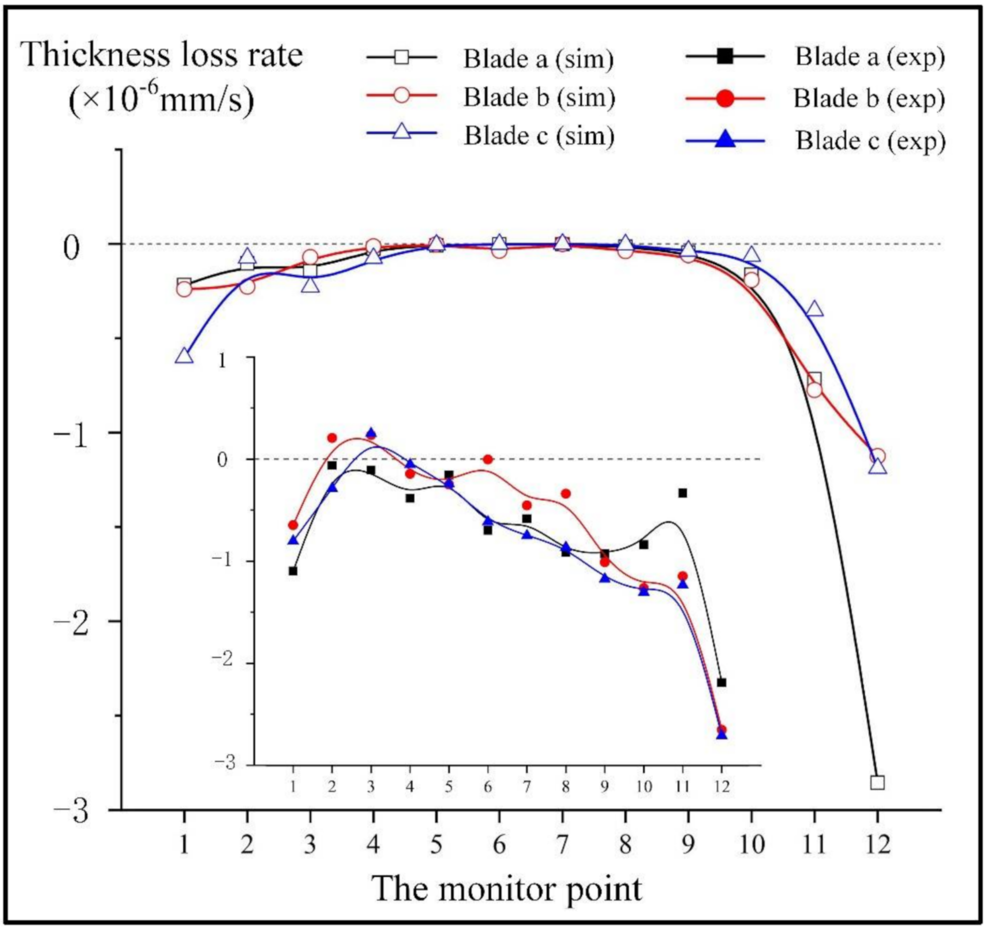

Figure 13. The thickness loss of the impeller at 1% concentration.

In Figure 13, the thickness loss was measured in the experiment and simulation. In order to be able to compare the two situations, the thickness loss rate was calculated by dividing the thickness loss by time, respectively.

It can be seen from Figure 13 that both in the experiment and simulation, at the measuring point near the blade leading edge (monitor point 1), the three blades all had serious thickness loss. When the measuring point is gradually moving away from the blade leading edge (at the monitor points 2 and 3), the thickness increases to a certain extent due to particle impact in the experiment. As the measuring point moves to the root of the impeller, the thickness loss gradually becomes serious.

The location of the largest thickness loss in the experimental wear is at the tail of the blade. The wear value of the three blades at the monitoring point 12 has an average increase of 215.53% compared to the wear value of the monitoring point 1.

It can be seen from Figure 13 that the thickness loss rate trend of the simulation is consistent with the experimental data, and the most severely worn point is 12 at the tail of the blades. For the blades b and c, the wear of the monitoring point 12 and the wear of the monitoring point 1 increased by an average of 232.35%, which is consistent with the experimental results.

The thickness loss in the experiment situation was greater than that in the simulation. The experimental value has a large fluctuation amplitude, which is due to the change of the impeller surface due to wear, and there are preliminary slight wear streaks.

In order to better explain the occurrence of wear, the streamline and the velocity distribution of the flow field were analyzed with the cascade diagram.

It can be seen from Figure 14 that the vortex and the corresponding flow chaotic position at the same concentration basically appeared in the middle area of the blade pressure surface, and the flow chaotic vortex always existed no matter how the position of the cascade section changed. Taking the 1% particle concentration as an example, it could be seen that when the span value near the blade tip was 0.1, the streamline was relatively smooth, the streamline vortex was mainly concentrated in the middle of the blade pressure surface and the position of the leading edge of the blade, and the streamlines in the three flow passages of ABC were similar. With the continuous increase of the span value (that is, corresponding to different sections from the tip to the root of the blade), it could be clearly seen that for the flow lines in each flow passage, a certain degree of difference gradually appeared, but the phenomenon of vortex near the pressure surface still existed. The particles at the pressure surface might have been affected by the flow field and repeatedly impacted the pressure surface. At the same time, the circumferential velocity of the pressure surface had a certain difference with the particles too, so the wear had to start from the end of the pressure surface with the highest circumferential velocity and gradually spread to the entire pressure surface.

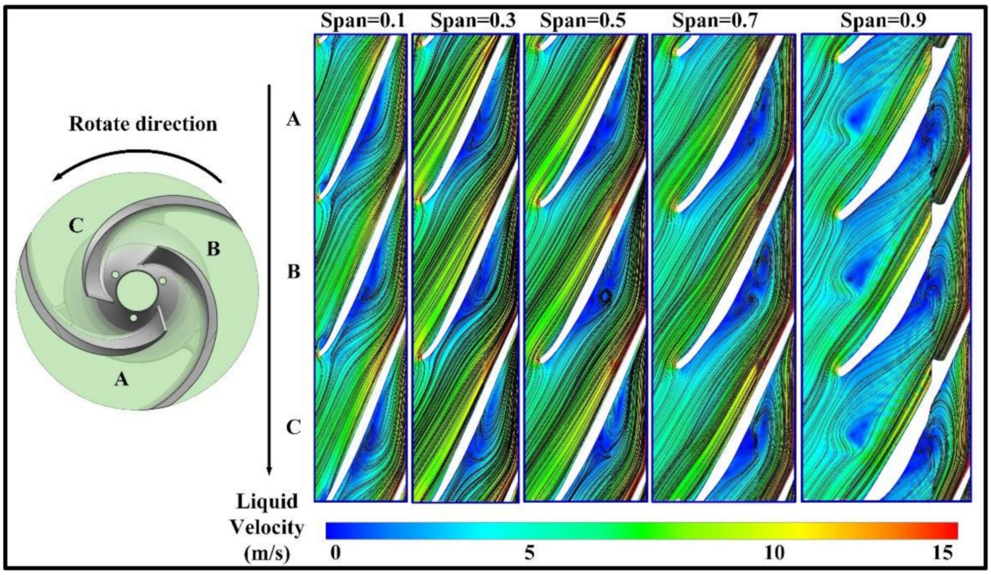

Figure 14. The blade-to-blade region of flow field velocity and streamline inside the impeller.

3.2. Internal Flow Field Analysis

When the centrifugal pump performed solid–liquid two-phase transportation, the presence of particles had a great impact on the flow field, and the change of the flow field in turn affected the movement and distribution of the particles, which in turn affected the mixed transport performance and wear. The flow field of the two-phase conveying condition and the flow field of the pure liquid conveying condition were compared in order to explore the influence of the particles on the flow field.

It can be seen from Figure 15 that in the liquid flow condition, the streamlines in the flow field appeared to be very smooth, and there was no particularly obvious vortex. At the same time, the cloud atlas of the flow field changed uniformly in this case. In the two-phase flow condition, it was obvious that there was a vortex near the pressure surface in the middle of the passage, and the closer the position was, the larger the vortex was. At the same time, when the span value was 0.9, which was the closest to the bottom of the blade, another vortex appeared near the leading edge of the blade. It could be seen from the velocity distribution of the flow field that as the section position gradually moved from the top to the bottom of the blade, the velocity of the flow field gradually decreased, the vortex range became larger, and another vortex even appeared near the bottom of the blade.

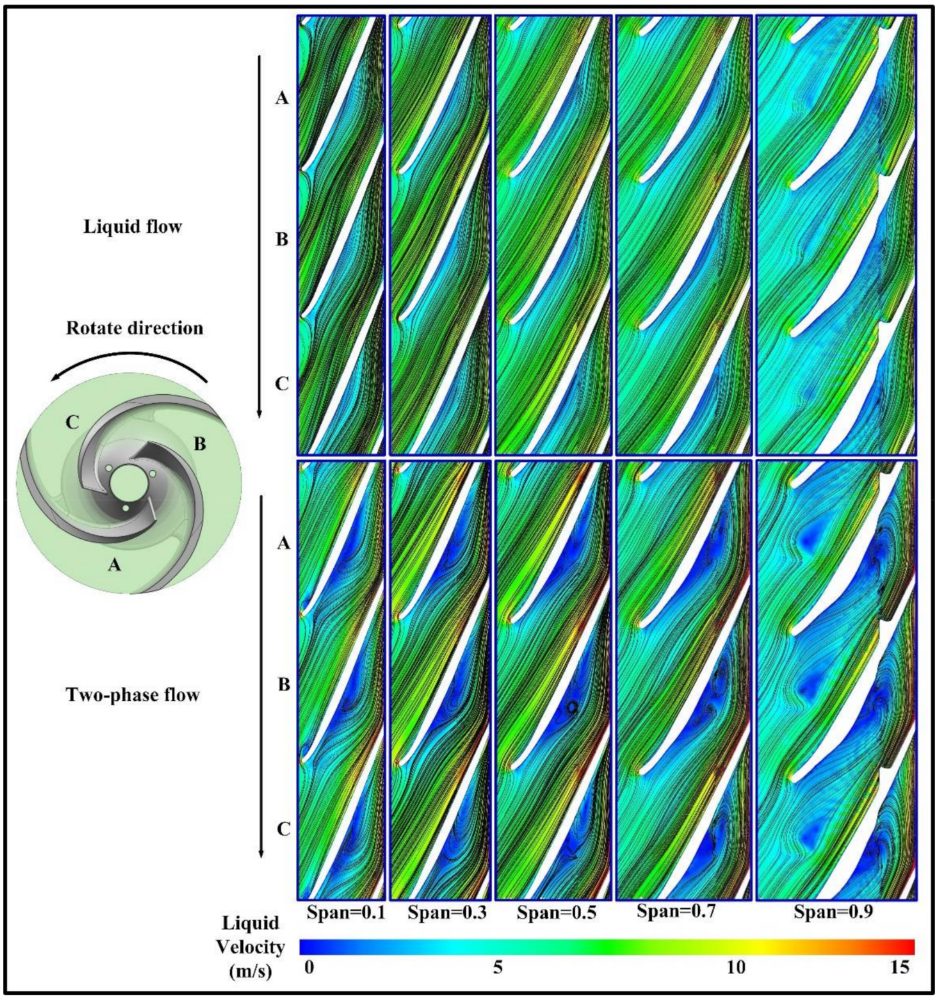

Figure 15. The difference in two-phase flow and liquid flow.

In order to further study the influence of the particles on the energy loss of the flow field, the energy gradient theory [16,17] was introduced for flow analysis.

The expression of the energy gradient, K [18], in the centrifugal pump was:

$$K = \frac{\sqrt{\mu_i^2}\sqrt{\left.\frac{\partial E}{\partial n}\right|_i^2}}{\sqrt{\mu_i^2}\sqrt{\left.\frac{\partial E}{\partial s}\right|_i^2} + \phi}, \quad (14)$$

In this expression, K is defined as the energy gradient function, μ is the velocity, E is the total mechanical energy, $\frac{\partial E}{\partial \mathrm{n}}$ is defined as the normal gradient of the total mechanical energy in the streamline, and $\frac{\partial E}{\partial \mathrm{s}}$ is defined as the flow gradient of the total mechanical energy. In this fraction, the denominator term is the flow gradient of the work carried out by the viscous shear stress in the streamline direction, which can be further expressed as the sum of the viscous friction loss of the total mechanical energy in the streamline direction and the energy dissipation function, ϕ.

The energy dissipation function, ϕ, can be defined as:

$$\phi = 2\rho\mu_t [\frac{1}{2}(\frac{\partial \mu_j}{\partial x_i} + \frac{\partial \mu_i}{\partial x_j})]^2, \tag{15}$$

The energy gradient theory could be used to predict the increase or loss of the flow field energy and the K value could be approximated as the ratio of the energy increase to the energy loss. To make it easier to observe, the logarithm lg$K$ of the K function was used for the display. It was defined that lg$K$ in the range of -0.3 to 0.3 meant that the local energy loss was equal to the energy increase. When lg$K \geq 0.3$, the energy increase was dominant, and lg$K \leq -0.3$ indicated that the energy loss was dominant. The energy change trend of the flow field reflected the corresponding energy change trend of the particles, which could be used to predict particle distribution and the movement to a certain extent. At the same time, the flow field tended to flow from a position with higher energy to a position with relatively low energy. The field tended to flow in a more complicated manner in areas where the energy increase was dominant.

Due to the different positions of the flow passages at the current moment and the direction of gravity, the particle distribution in each flow passage and each span had to be different. In Figure 16, near the top of the blade, when the span values were 0.1 and 0.3, the high-concentration particle volume fraction appeared at the entrance of the C flow passage. This was because the particles were gradually sinking, they were affected by gravity before entering the front of the impeller zone, and the inlet of the C flow channel was just below the flow passage at that moment. At that time, a large number of particles entered the C flow channel. In the particle distribution diagram, it can also be seen that as the span value increased, the particles were concentrated at the entrance from the beginning and they gradually spread to the entire flow passage. At the same time, the particle volume fraction in front of the pressure of the B channel increased with the increase of the cross-sectional span value, and most of the particles were free near the bottom of the blade pressure surface, which led to the wear of the blade pressure surface, as shown in Figure 11. When the span value was 0.9, close to the wall of the impeller hub, there were a large number of particles in the wall and a large amount of the volume was occupied. This was also the reason that the wear of the hub could spread to the entire wall.

It could be seen from the distribution of lg$K$ in Figure 16 that when the span value was 0.1, there was a large range of high-energy areas in each flow passage, mainly concentrated in the center of the suction surface and close to the impeller outlet area, and there was almost no position where the energy was weakened. It could be known from the particle distribution that the particles had not completely entered the flow passage when the span value was 0.1. At other span values, areas where the energy was weakened gradually appeared, and particles also began to enter the flow passage. This indicated that the main reason for the energy weakening of the flow field was the existence of particles, and the flow field drove the movement of particles by transferring energy to the particles.

Combined with the current concentration situation and the distribution of lg$K$ on the sections with different span values, it could be known that when the span value was 0.1, the flow field had a large range of high-energy regions. As the span value continued to rise (that is, corresponding to the section from the tip to the root of the blade), it could be clearly observed that the high-energy area gradually decreased, while the energy balance area occupies most of the flow passage. According to the characteristics that fluids tend to flow from high-energy regions to low-energy regions, it could be considered that in the vertical scale, the flow field continuously flowed from the tip to the root of the blade, which also made most of the particles receive energy transfer in the impeller flow passage. Thereby, the particles continuously accumulated in the root area of the blade, and since most of the energy of the flow field was in the equilibrium range near the root of the blade, the particle concentration in that area was relatively higher.

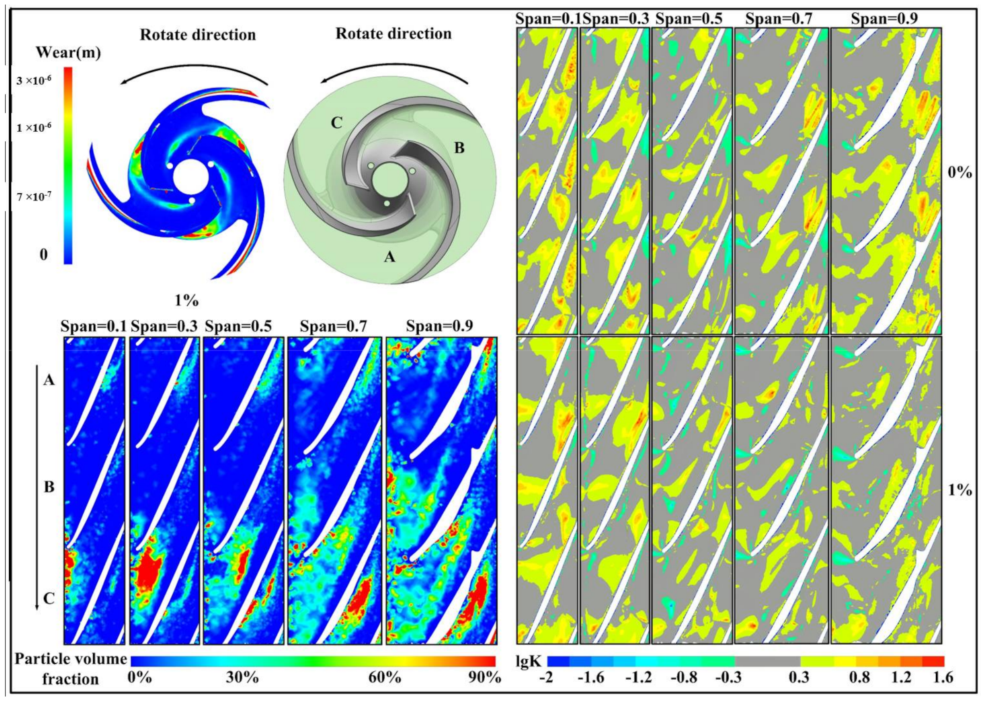

Figure 16. The difference in two-phase flow and liquid flow.

In order to understand the influence between the particles and the flow field, the lg$K$ distributions of both conditions were compared. When the span values were 0.1 and 0.3, it could be seen that the energy increase was dominant (lg$K \geq 0.3$) and it mainly appeared in the middle of the flow passage, and most of the energy increase area had a certain distance from the pressure surface and were close to the suction surface. This was also similar to the condition of the water. It could be known that due to the presence of particles in the current cascade section, the energy transferred to the particles by the flow field was relatively small, and the energy gradient distribution in the three flow passages was relatively similar.

However, in the area where the span value was 0.5, significant differences began to appear for the conditions of 0% and 1% mass concentrations. The exit position of the flow passage was in the area of reduced energy for the condition of clear water, but when there were particles, either it completely disappeared, or the energy increase was dominant. This might have been because the particles further transferred their own energy to the flow field at the current position.

In the section near the root of the blade (span values of 0.7 and 0.9), the difference between 0% and 1% particles was more obvious, especially when the span value was 0.9. The entire flow passage basically had the energy increase dominate for the condition of water, but when particles existed, the energy increase dominated the area in the flow passage that appeared near the suction surface.

By analyzing the overall flow characteristics of the flow passage, it could be found that compared with the K value in the flow passage for the condition of clear water transportation, the K value of the particle aggregation area during two-phase transportation was relatively smaller. The area near the root of the blade with the most particles (the span value was 0.9) had the most significant decrease in the K value. Since the K value could indicate the local energy situation, a small K value meant that this was a low-energy area, and the flow was relatively stable, so the particles aggregated there.

The flow loss in the impeller channel mainly included the boundary layer flow loss and the main channel flow loss. It could be found that a certain number of particles near the wall could disturb the boundary layer during solid–liquid two-phase transportation, reducing its thickness and thereby reducing the boundary layer flow loss. However, when the concentration was too high, the presence of particles caused the overall flow field disturbance, which led to an increase of the main channel flow loss. Therefore, combined with the head curve of the centrifugal pump in Figure 4, it could be found that at low concentrations, the reduction of the boundary layer flow loss was dominant, so the head change of the solid–liquid two-phase flow was small. After the increase in concentration, the decrease in the boundary layer flow loss was no longer sufficient to compensate for the increase in the main channel flow loss, which led to an increase in the flow loss in the impeller flow channel, so the head was greatly reduced.

4. Conclusions

By comparing the numerical simulation results and experimental results of the centrifugal pump in solid–liquid mixed transportation, the following conclusions were drawn:

1. It can be known from the performance of the centrifugal pump that in the experiment with the same flow rate, the presence of particles will reduce the head and efficiency of the centrifugal pump, but the shaft power change was relatively small. As the concentration increases, the head and efficiency will further decrease. When the concentration increased to 6%, the head decreased by 14% and the efficiency decreased by 18%.
2. The most severely worn parts were the impeller hub and the leading edge of the blade. The abrasion of the hub wall surface started from the wall surface farthest from the rotating shaft and gradually spread to the entire hub wall surface. The wear of the pressure surface gradually spread to the entire pressure surface from the region near the root of the blade. Through the analysis of the streamline and energy gradient, it could be known that the particles were affected by their own initial velocity and the flow field after colliding with the impeller, and they continued to gather towards the root of the blade. However, since the wall surface farthest from the axis had the largest relative velocity for the particles, the wear on the wall surface of the hub started from the wall surface the farthest away first and the pressure surface began to wear from the end of the root blade.
3. The leading edge of the blade was mainly affected by impact wear. When the concentration increased and the number of particles gradually increased, the leading edge of the blade even appeared to be twisted to a certain extent. It could be seen from the simulation results that the particles directly impacted the leading edge of the blade to cause impact wear, and the simulation results of the wall wear trend were consistent with the experimental situation.
4. The energy increase of the flow field mainly occurred in the middle of the flow passage close to the tip of the blade, and the position of the energy loss mainly occurred in the center of the flow field close to the pressure surface. Most of the flow passage near the root was energy-balanced. The distribution of the energy gradient function, K, generally maintained a gradual decrease from the tip to the root of the blade, which showed that the flow in the pump continuously pushed the particles to sink on the vertical scale. Additionally, since most of the energy of the flow field was in the equilibrium range near the root, the particle concentration at the blade root was relatively high.

Author Contributions: Conceptualization, Z.J. and Y.L.; Data curation, Z.J. and X.Z.; Formal analysis, Z.J.; Funding acquisition, Y.L.; Investigation, Z.J.; Methodology, Z.J. and Y.L.; Project administration, Y.L.; Resources Y.L.; Software, Z.J.; Supervision, Y.L.; Validation, Z.J. and X.Z.; Writing—original

draft, Z.J.; Writing—review and editing, Y.L. All authors have read and agreed to the published version of the manuscript.

Funding: This work was supported by the National Natural Science Foundation of China (No. 51976197), and the Key Research and Development Program of Zhejiang Province (No. 2020C03099).

Data Availability Statement: The data presented in this study are available on request from the corresponding author. Due to the huge amount of data, it is not convenient to save at publicly archived datasets.

Conflicts of Interest: The authors declare no conflict of interest.

References

1. Khalid, Y.A.; Sapuan, S.M. Wear analysis of centrifugal slurry pump impellers. *Ind. Lubr. Tribol.* **2007**, *59*, 18–28. [CrossRef]
2. Wang, Z.; Qian, Z. Effects of concentration and size of silt particles on the performance of a double-suction centrifugal pump. *Energy* **2017**, *123*, 36–46. [CrossRef]
3. Ravelet, F.; Bakir, F.; Khelladi, S.; Rey, R. Experimental study of hydraulic transport of large particles in horizontal pipes. *Exp. Therm. Fluid Sci.* **2013**, *45*, 187–197. [CrossRef]
4. Zouaoui, S.; Djebouri, H.; Mohammedi, K.; Kheladi, S.; Aider, A.A. Experimental study on the effects of big particles physical characteristics on the hydraulic transport inside a horizontal pipe. *Chin. J. Chem. Eng.* **2016**, *24*, 317–322. [CrossRef]
5. Zhao, W.; Zhao, G. Numerical investigation on the transient characteristics of sediment-laden two-phase flow in a centrifugal pump. *J. Mech. Sci. Technol.* **2018**, *32*, 167–176. [CrossRef]
6. Qian, Z.; Wang, Z.; Zhang, K.; Wu, Y.; Wu, Y. Analysis of silt abrasion and blade shape optimization in a centrifugal pump. *Proc. Inst. Mech. Eng. Part. A J. Power Energy* **2014**, *228*, 585–591. [CrossRef]
7. Pagalthivarthi, K.V.; Gupta, P.K.; Tyagi, V.; Ravi, M.R. CFD prediction of erosion wear in centrifugal slurry pumps for dilute slurry flows. *J. Comput. Multiph. Flows* **2011**, *3*, 225–245. [CrossRef]
8. Shen, Z.J.; Li, R.N.; Han, W.; Zhao, W.G.; Wang, X.H. The research on particle trajectory of solid-liquid two-phase flow and erosion predicting in screw centrifugal pump. *IOP Conf. Ser. Mater. Sci. Eng.* **2016**, 129. [CrossRef]
9. Tarodiya, R.; Gandhi, B.K. Experimental investigation of centrifugal slurry pump casing wear handling solid-liquid mixtures. *Wear* **2019**, 434–435. [CrossRef]
10. Kaushal, D.R.; Thinglas, T.; Tomita, Y.; Kuchii, S.; Tsukamoto, H. CFD modeling for pipeline flow of fine particles at high concentration. *Int. J. Multiph. Flow* **2012**, *43*, 85–100. [CrossRef]
11. Huang, S.; Huang, J.; Guo, J.; Mo, Y. Study on wear properties of the flow parts in a centrifugal pump based on EDEM–fluent coupling. *Processes* **2019**, *7*, 431. [CrossRef]
12. Cai, X.; Zhou, S.P.; Li, S. Study on the influence of back blade shape on the wear characteristics of centrifugal slurry pump. *IOP Conf. Ser. Mater. Sci. Eng.* **2016**, *129*, 4047–4057. [CrossRef]
13. Grant, G.; Tabakoff, W. Erosion prediction in turbomachinery resulting from environmental solid particles. *J. Aircr.* **1975**, *12*, 471–478. [CrossRef]
14. Ahlert, K.R. *Effects of Particle Impingement Angle and Surface Wetting on Solid Particle Erosion of AISI 1018 Steel*; The University of Tulsa: Tulsa, OK, USA, 1994.
15. Li, Y.; Zhang, H.; Lin, Z.; He, Z.; Xiang, J.; Su, X. Relationship between wear formation and large-particle motion in a pipe bend. *R. Soc. Open Sci.* **2019**, *6*, 181254. [CrossRef] [PubMed]
16. Dou, H.-S. A Universal Equation for Calculating the Energy Gradient Function in the Energy Gradient Theory. *arXiv* **2016**, arXiv:1610.01517.
17. Dou, H.-S. Mechanism of flow instability and transition to turbulence. *Int. J. Non Linear Mech.* **2006**, *41*, 512–517. [CrossRef]
18. Chen, X.; Zhu, Z.; Dou, H.-S.; Li, Y. Large eddy simulation of energy gradient field in a centrifugal pump impeller. *Proc. Inst. Mech. Eng. Part. C J. Mech. Eng. Sci.* **2018**, *233*, 4047–4057. [CrossRef]